Track-Pattern-Based Model for Seasonal Prediction of Tropical Cyclone Activity in the Western North Pacific

HYEONG-SEOG KIM* AND CHANG-HOI HO

School of Earth and Environmental Sciences, Seoul National University, Seoul, South Korea

JOO-HONG KIM

Department of Atmospheric Sciences, National Taiwan University, Taipei, Taiwan

PAO-SHIN CHU

Department of Meteorology, University of Hawaii at Manoa, Honolulu, Hawaii

(Manuscript received 4 May 2011, in final form 20 December 2011)

ABSTRACT

Skillful predictions of the seasonal tropical cyclone (TC) activity are important in mitigating the potential destruction from the TC approach/landfall in many coastal regions. In this study, a novel approach for the prediction of the seasonal TC activity over the western North Pacific is developed to provide useful probabilistic information on the seasonal characteristics of the TC tracks and vulnerable areas. The developed model, which is termed the ''track-pattern-based model,'' is characterized by two features: 1) a hybrid statistical–dynamical prediction of the seasonal activity of seven track patterns obtained by fuzzy *c*-means clustering of historical TC tracks and 2) a technique that enables researchers to construct a forecasting map of the spatial probability of the seasonal TC track density over the entire basin. The hybrid statistical–dynamical prediction for each pattern is based on the *statistical* relationship between the seasonal TC frequency of the pattern and the seasonal mean key predictors *dynamically* forecast by the National Centers for Environmental Prediction Climate Forecast System in May. The leave-one-out cross validation shows good prediction skill, with the correlation coefficients between the hindcasts and the observations ranging from 0.71 to 0.81. Using the predicted frequency and the climatological probability for each pattern, the authors obtain the forecasting map of the seasonal TC track density by combining the TC track densities of the seven patterns. The hindcasts of the basinwide seasonal TC track density exhibit good skill in reproducing the observed pattern. The El Niño–/La Niña–related years, in particular, tend to show a better skill than the neutral years.

1. Introduction

Every year, many coastal areas suffer from large social and economic damage caused by tropical cyclone (TC)-induced gusts and downpours. The seasonal prediction of the TC activity has been an important issue for TC-prone countries in their efforts to mitigate the potential losses from TCs in the coming TC season, which, indeed, is gradually becoming as important as real-time forecasts of the track and intensity of TCs. Many pioneering attempts were made to develop a seasonal prediction model for the basinwide TC activity in various TC-prone ocean basins, such as Nicholls (1979) in the Australian region, Gray (1984) in the Atlantic basin, and Chan et al. (1998) in the western North Pacific (WNP) basin. The statistical prediction models were mostly developed using empirical relations between the target TC activity and the preceding large-scale environments that are considered to be influential. The prototype statistical prediction models have been improved by follow-up studies, and some new models have been developed as well (e.g., Gray et al. 1992, 1993, 1994; Elsner and Schmertmann 1993; Hess et al. 1995; Chan et al. 2001; Klotzbach and

* Current affiliation: Atmospheric and Oceanic Science, Princeton University, and NOAA/Geophysical Fluid Dynamics Laboratory, Princeton, New Jersey.

Corresponding author address: Dr. Joo-Hong Kim, Department of Atmospheric Sciences, National Taiwan University, No. 1, Section 4, Roosevelt Road, Taipei 106, Taiwan.
E-mail: jhkim004@gmail.com

DOI: 10.1175/JCLI-D-11-00236.1

Gray 2004; Chu and Zhao 2007). By virtue of these efforts, the prediction of basinwide seasonal TC activity has been continuously improved so that some of them could be applied as operational prediction schemes.

There has been another development trend that confines the forecasting target region to the near coastal area for the purpose of providing more reliable information about regional TC landfalls (e.g., Saunders and Lea 2005; Elsner and Jagger 2006). With regard to the WNP to which many TC-prone countries are adjacent, there has been a thrust to develop seasonal prediction models for the subbasin-scale TC activity—for example, the South China Sea (Liu and Chan 2003), the East China Sea (Ho et al. 2009a; H.-S. Kim et al. 2010), Taiwan (Chu et al. 2007, 2010; Lu et al. 2010), and Korea (Choi et al. 2009). These studies showed that skillful forecasts of the regional TC activity are possible through statistical relations with some antecedent large-scale environmental predictors. However, it should be noted that the statistical relations applied to any statistical model are exclusive with respect to the specific TC activity concerned. Accordingly, the models must be independently developed to make predictions for unexplored regions.

Apart from the statistical predictions, dynamical prediction has also been attempted using numerical models (e.g., Vitart et al. 2007; Camargo and Barnston 2009; Zhao et al. 2010). The innovative dynamic core and physics schemes with increasing horizontal and vertical resolution in state-of-the-art dynamic models lead to the dynamical prediction skill of basinwide TC activity comparable to the statistical models. However, the dynamical seasonal prediction of regional TC activity or TC landfall is still challenging because the simulation of TC tracks is rather unreliable in climate models (Camargo et al. 2006), which will very likely be improved in the next-generation climate forecast systems.

The objective of this study is to develop a novel seasonal prediction technique that aims at producing a probabilistic map of seasonal TC occurrences for the entire WNP basin. To accomplish this objective, a track-pattern-based model is devised based on a finite number of representative patterns of WNP TC tracks. The possibility of track-pattern-based prediction for the seasonal TC activity was discussed in Camargo et al. (2007) and Kim et al. (2011) in which the TC tracks were numerically clustered into several patterns. Recently, Chu et al. (2010) developed a track-pattern-based statistical prediction model for the seasonal TC frequency near Taiwan and argued that the track-pattern-based approach would provide a more physical understanding of the forecasting skills. Extending from a purely statistical track-pattern-based approach targeted for a limited domain (Chu et al. 2010), this study uses predictors from a dynamical model for predicting the spatial distribution of seasonal TC tracks over the entire WNP basin. The proposed model can be classified as a hybrid statistical–dynamical type (e.g., Wang et al. 2009; Kim and Webster 2010; Vecchi et al. 2011) because it is based on the *statistical* relations between the interannual variability of the TC frequency in each track pattern and some *physically relevant concurrent* seasonal large-scale environments from the *dynamical* ensemble seasonal forecasts of the National Centers for Environmental Prediction (NCEP) Climate Forecast System (CFS). After the statistical predictions are made for each track pattern, the seasonal TC track density map is constructed using a reasonable combining technique.

This paper is organized as follows. Section 2 describes the datasets used in this study. Section 3 presents the technical procedure of the track-pattern-based hybrid statistical–dynamical prediction model. Section 4 discusses the validation of the prediction model. Finally, the concluding remarks are given in section 5.

2. Data

The information on the TC locations is taken from the best-track dataset archived by the Regional Specialized Meteorological Centers Tokyo-Typhoon Center. This dataset contains 6-hourly latitude and longitude locations, minimum central pressure, maximum sustained wind speed, etc. Here, we used only the TC locations with maximum sustained wind speed greater than 17 m s^{-1}. The analysis is targeted at the TCs formed during June–October (JJASO, the TC season) covering approximately 80% of the annual TCs over the WNP.

The NCEP CFS retrospective forecasts (Saha et al. 2006) are used to provide seasonal large-scale information for developing the hybrid statistical–dynamical model based on the track patterns. The NCEP CFS, which is a fully coupled dynamical prediction system, provides 9-month atmospheric/oceanic forecast fields for every month since 1981.[1] The model diagnostics of the atmospheric model, such as wind fields, are provided with a horizontal resolution of 2.5° × 2.5° (latitude–longitude) whereas those of the oceanic model, such as sea surface temperature (SST), have a horizontal resolution of 1° × 2°. These data were used in the hybrid

[1] The initial conditions for 1981–90 CFS retrospective forecast version 1 in the NCEP Climate Prediction Center (CPC) Web site contained a treatment that was inconsistent with that after 1990. The CPC reran the hindcasts with corrected initial condition for 1981–90, primarily for real-time operational forecast calibration (W. Wang 2011, personal communication). This study utilizes the updated data.

statistical–dynamical model for predicting the seasonal Atlantic hurricane frequency (Wang et al. 2009). To obtain the dynamic forecasts during JJASO, we use 15 ensemble members of the NCEP CFS forecasts, which were run using different initial conditions prior to the TC season. The 15 initial conditions can be classified into three groups, each of which consists of 5 consecutive days centered on 11 and 21 April and 1 May.

This study also utilizes the monthly mean atmospheric fields from the NCEP Reanalysis-2 (Kanamitsu et al. 2002) and the monthly mean SST from the NOAA optimum interpolation SST version 2 (Reynolds et al. 2002). The NCEP Reanalysis-2 and the NOAA SST are provided with horizontal resolution of $2.5° \times 2.5°$ and $2° \times 2°$, respectively. The NCEP atmospheric fields used include the 850-hPa relative vorticity, 850-hPa and 200-hPa horizontal winds, and 50-hPa zonal wind. All of these observational datasets are applied to validate the NCEP CFS forecasts and to verify the potential predictors from the NCEP CFS forecasts.

3. Model description

Figure 1 illustrates the process of the seasonal prediction model developed in this study. As a first step, the representative TC track patterns are required so as to proceed to the next step because they are the primary basis of this track-pattern-based model. In the second step, the seasonal TC frequencies of each track pattern are separately predicted using an empirical statistical prediction method in which dynamic environmental predictors are incorporated. Owing to this step, the model is classified as a hybrid statistical–dynamical type of model. The final step is to construct the forecasting map of TC track density by combining the prediction results of each cluster. During this step, the spatial probability of each track pattern obtained from the climatology is applied as the base, which is required to create the forecasting map.

a. TC track patterns

To obtain the basic patterns of TC tracks, the fuzzy *c*-means clustering method is adopted as a numerical clustering technique (Kim et al. 2011). The fuzzy *c*-means clustering method can yield reasonable clusters even with a complex input dataset such as TC tracks in which the cluster boundaries are not distinct. Kim et al. (2011) introduced a straightforward method to incorporate the entire shapes of all TC tracks into the fuzzy *c*-means clustering algorithm by interpolating all tracks into equal number of segments. With several cluster validity measures to determine the optimal number of clusters, seven representative patterns of TC tracks were obtained using

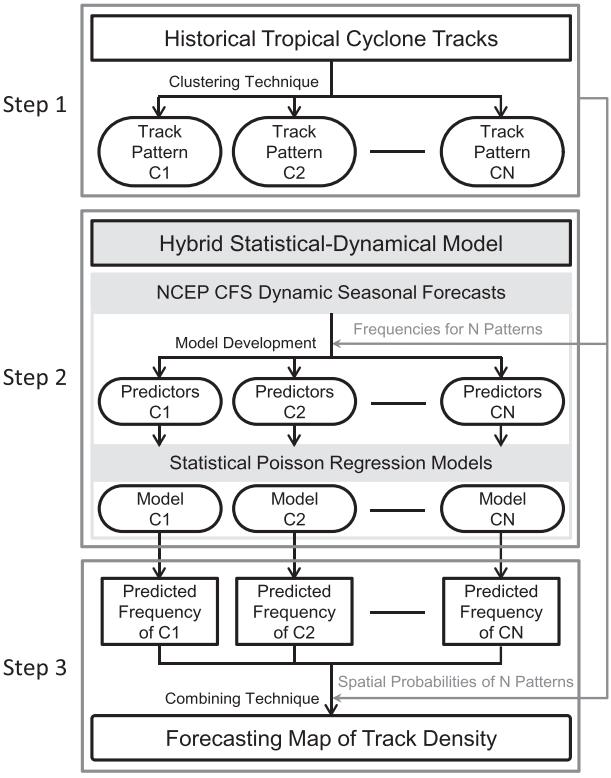

FIG. 1. Schematic for the track-pattern-based prediction model.

the TCs during JJASO for the period 1965–2006.[2] The fuzzy clustering algorithm allows each TC track to belong to all clusters with different membership degrees. In this study, however, the tracks are allocated into one cluster in which membership degree is the largest (i.e., hard partitioning). Chu et al. (2010) also applied the fuzzy *c*-means clustering method to the JJASO TCs during 1979–2006 and obtained the similar seven patterns. These patterns were also obtained by Camargo et al. (2007), though the clustered patterns were somewhat different from those of Kim et al. (2011) because the annual TCs during 1950–2002 were used. All of these studies indicate that seven could be a characteristic number of track patterns over the WNP.

Figure 2 illustrates the seven patterns (C1–C7) of TC tracks during JJASO of 1965–2006.[3] While the TCs in C1 form over the northwest Philippine Sea and move to Korea and Japan (Fig. 2a), those in C2 develop over the southeast WNP and move mostly to Japan with long

[2] The power of the fuzziness coefficient is set to 2, and the Euclidean norm is used for the dissimilarity of the fuzzy objects. Detail description of fuzzy clustering for the TC tracks is given in Kim et al. (2011).

[3] Fig. 2 is identical to Fig. 4 in Kim et al. (2011).

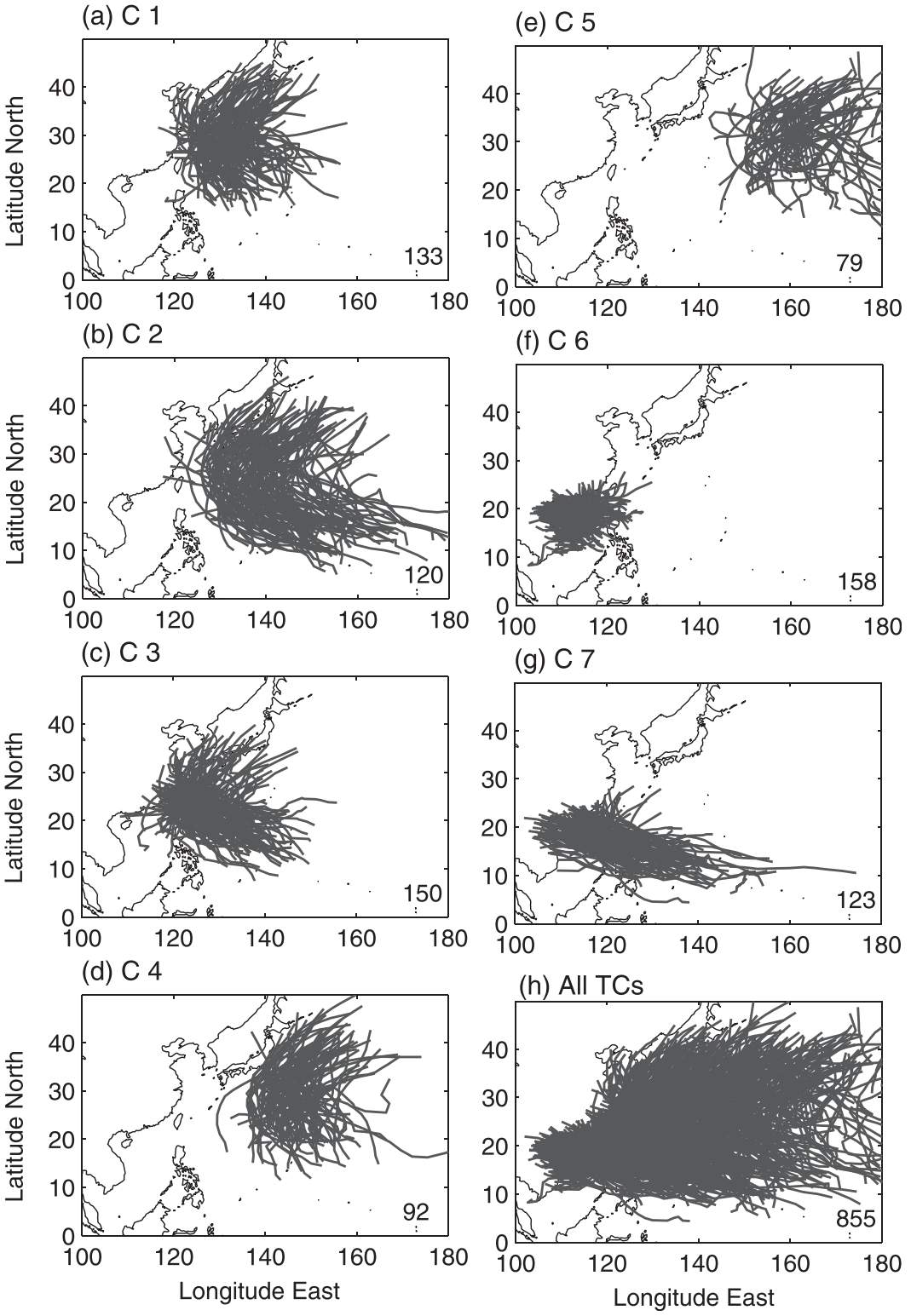

FIG. 2. (a)–(g) Seven track patterns and (h) all the tracks of TCs over the WNP and their frequencies during the TC seasons for the period 1965–2006.

trajectories (Fig. 2b). These two patterns are representative of typical modulation of the El Niño–Southern Oscillation (ENSO) (Wang and Chan 2002; Ho and Kim 2011). Most TCs in C3 strike Taiwan and East China with west-oriented tracks (Fig. 2c) and those in C4 pass east of Japan with early recurving tracks (Fig. 2d). It has been suggested that the C3- and C4-type TCs are possibly related to the central Pacific (CP)–El Niño (also known as El Niño Modoki) and the stratospheric quasi-biennial oscillation (QBO), respectively (e.g., Ho et al. 2009b; J.-H. Kim et al. 2010; Kim et al. 2011). C5 contains TCs traveling the easternmost oceanic area with irregular shapes (Fig. 2e). C6 consists of TCs formed over the South China Sea (Fig. 2f), whereas C7 represents straight-moving TCs across the Philippines (Fig. 2g). The latter three patterns were classified as those reflecting the effect of local environments such as SST and steering flows (Kim et al. 2011).

As mentioned above, C1, C2, C3, and C4 reflect the influences of La Niña, El Niño, El Niño Modoki, and QBO, respectively. To confirm these relations, the correlations of TC frequency and relevant oscillation indices during the TC season are examined with regard to each pattern. The correlation analysis uses the period 1981–2006, which is the main analysis period of this study. The correlation coefficients for C1 and C2 with the Niño-3.4 index during JJASO are −0.43 and 0.74, respectively. On the other hand, the correlation coefficient for C3 with the El Niño Modoki index (Ashok et al. 2007) during JJASO is 0.5 and that for C4 with the 50-hPa QBO index during JJASO reaches −0.70. All correlation coefficients are statistically significant at the 95% confidence level, as shown by a two-tailed t test, suggesting the feasibility of seasonal prediction of these track patterns based on large-scale environments. It should be noted that the relations are simultaneous rather than time lagged. We checked the time-lagged correlation coefficients with the preseason indices (i.e., December to May) but only found low and insignificant values. The larger simultaneous correlation values justify the use of the NCEP CFS large-scale environments during JJASO as potential predictors.

b. *Hybrid statistical–dynamical prediction model*

The hybrid statistical–dynamical technique is employed for the seasonal prediction of each track pattern. The hybrid statistical–dynamical prediction model is developed on the basis of the empirical relationship between the observed TC frequency and the dynamically predicted large-scale environments during the same period (Wang et al. 2009; Kim and Webster 2010), unlike the statistical prediction models that adopt the relevant antecedent large-scale environments as predictors (Gray et al. 1992; Chan et al. 2001; Chu and Zhao 2007; and many others). Because the simultaneous large-scale environments are better correlated with the track patterns, the hybrid statistical–dynamical prediction method may, in principle, yield more skillful prediction. If the dynamic model forecasts provide realistic large-scale environments during the target season, the hybrid-type approach can give a more reliable prediction; otherwise, its forecast skill may degrade.

To select the potential predictors for each pattern, we analyze the correlations between the seasonal TC frequency of each pattern and several large-scale environments from observations and NCEP CFS forecasts. Candidate variables for potential predictors are mostly limited to SST, magnitude of the vertical wind shear (VWS) between 200 and 850 hPa, 850-hPa relative vorticity (VOR_{850}), and 200-hPa zonal wind (U_{200}); however, the 50-hPa zonal wind (U_{50}) appears to be amenable for C4, which is inversely correlated with the QBO (Ho et al. 2009b; Kim et al. 2011). Except for SST and U_{50}, the critical regions, which approximately enclose areas with significant correlations between TC frequencies and environmental predictors, is confined in and around the WNP basin (10°S–40°N, 90°E–150°W). All variables are averaged for JJASO.

Figure 3 illustrates the correlation maps between the seasonal TC frequency in C1 and the four predictor candidates from the observations (Figs. 3a–d) and the ensemble mean of the 15 NCEP CFS forecasts (Figs. 3e–h) during the period 1981–2006. For a sample size of 26 years, ±0.31 is the 90% significance level of the correlation coefficient with the two-tailed t test. With regard to the SST, negative correlations prevail over the tropical central and eastern Pacific, while positive correlations exist over the tropical western South Pacific and extratropical North and South Pacific (Fig. 3a), indicating that C1 is active during La Niña. In association with La Niña, the TC genesis region shifts toward the northwest Philippines Sea because of the anomalous low-level anticyclonic vorticity and the large vertical wind shear over the tropics associated with the weaker monsoon trough (Wang and Chan 2002). The local atmospheric responses to La Niña are well reflected in the correlation maps for VOR_{850}, U_{200}, and VWS (Figs. 3b–d).

For C1 the significantly correlated regions in the observations appear consistently in the ensemble mean of the NCEP CFS forecasts (Figs. 3e–h). Not only does this indicate that the NCEP CFS has substantial skill in predicting the characteristic large-scale environments influencing the interannual variability of the observed TC activity, but it also confirms the feasibility of the hybrid statistical–dynamical prediction for the TC track patterns using the NCEP CFS forecasts. According to

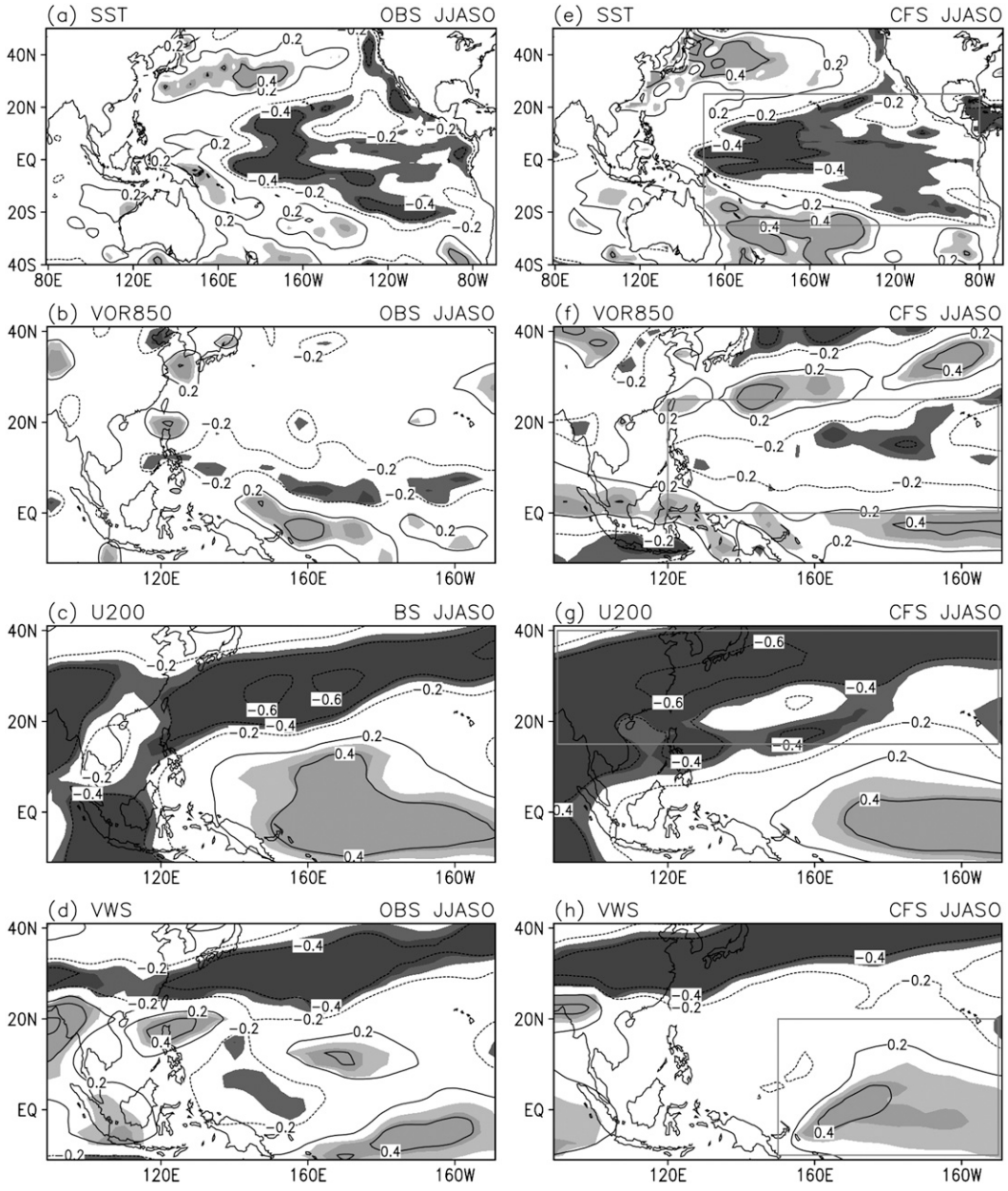

FIG. 3. Correlation coefficients between the TC frequency in C1 and the SST, 850-hPa vorticity (VOR_{850}), 200-hPa zonal wind (U_{200}), and absolute vertical wind ashear (VWS) in (a)–(d) the observations and (e)–(f) NCEP CFS forecasts during June–October for the period 1981–2006. The light (dark) shadings represent the positively (negatively) significantly correlated regions. The significance at the 95% confidence level is darker than that at the 90% confidence level. The boxes in the right panels denote the critical regions.

the two correlation patterns obtained from the ensemble mean of the NCEP CFS forecasts and actual observations, we select the critical regions wherein the key parameters are used for the final predictor sets (boxes in Figs. 3e–h). We also check the correlation between the NCEP CFS ensemble forecasts and the observation to understand how well the NCEP CFS predicts the environmental parameters over the selected region (Fig. 4). The mean correlation coefficients are 0.65 for SST, 0.68 for U_{200}, 0.63 for VWS, and 0.73 for VOR, respectively. All coefficients are significant at the 95% confidence level, suggesting that the NCEP CFS has good predictability of the ENSO-related environments. This also ensures that the NCEP CFS can serve the environmental predictors during the TC season for the hybrid statistical–dynamical model.

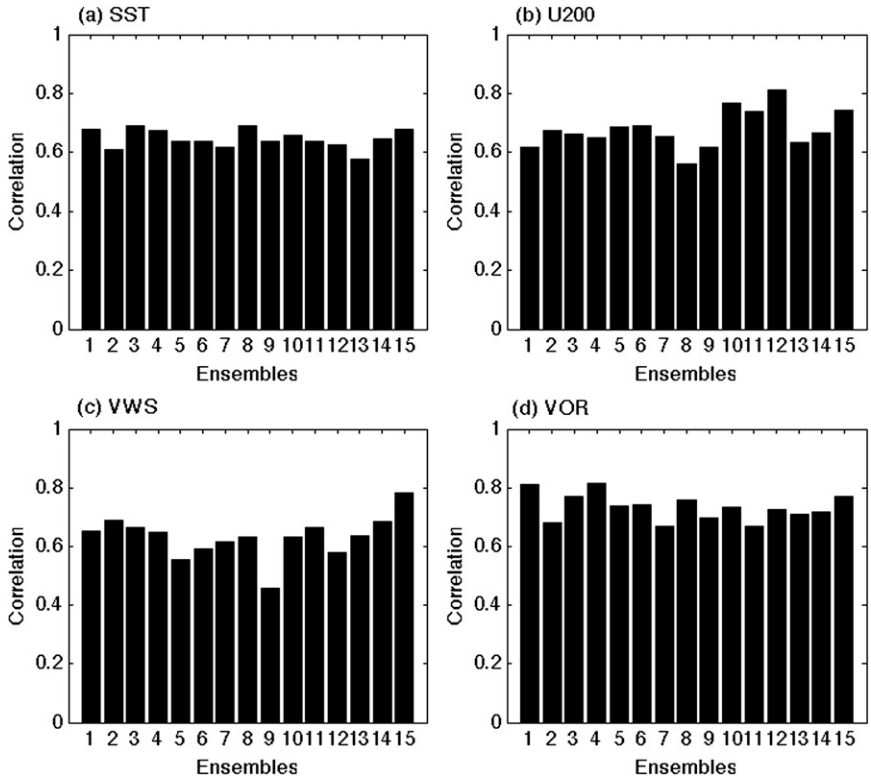

FIG. 4. Correlation coefficients between the observation and the NCEP CFS ensemble forecasts over the selected critical regions in Fig. 3.

The procedure used to determine critical regions for C2 is exactly the same as C1 but with an opposite sign, indicating mirrorlike patterns between La Niña and El Niño (not shown). The critical regions for C3, as shown in Fig. 5 (right column), are slightly different from those for C1 and C2 because C3 is related to the warming over the CP (Kim et al. 2011). For C1–C3 all of the candidate variables are kept as potential predictors. This is expected because El Niño and La Niña are known to have seasonally persistent influences on large-scale environments over the WNP. Accordingly, the critical regions for C1–C3 are relatively large. For C4, VOR_{850} is left as the only predictor among the four common variables (Fig. 6). However, because C4 is negatively correlated with the stratospheric QBO phase (Ho et al. 2009b; Kim et al. 2011), tropical U_{50} is selected as a special predictor variable. Due to the quasiperiodic nature of the QBO, the inclusion of U_{50} greatly enhances the predictability of C4 pattern (see Table 1). For the sake of simplicity, correlation patterns for C5–C7 will not be presented. Suffice to say that each one of them has its own critical regions.

Figure 7 summarizes the critical regions for each predictor according to track pattern from C1 to C7. Although the critical regions are defined using the ensemble mean of the NCEP CFS forecasts, the predictors are picked from the individual NCEP CFS ensemble members. Time series are obtained as final predictors by area averaging over the significantly correlated area for each ensemble member. Consequently, 15 predictor sets are obtained from the individual NCEP CFS forecasts. With these predictor sets, the hybrid statistical–dynamical model can provide 15 ensemble forecast members.

It is noted that the predictors for the ENSO-related clusters (i.e., C1, C2, and C3) are correlated with each other. Owing to the substantial influence of ENSO, it is difficult to find the chosen predictors that are entirely and physically independent of each other. To verify the use of the partly dependent predictors, we examine a variance inflation factor (VIF) for each ensemble predictor sets (Davis et al. 1986). The larger VIF means the higher multicollinearity. Generally, a value of 10 is used as the criteria (e.g., Davis et al. 1986; O'Brien 2007; Villarini et al. 2011). Among the VIFs for the predictors for the seven patterns, the maximum VIF value is found to be 7.01 for VWS for C1, suggesting that the predictors selected are acceptable for the model.

The statistical prediction technique adopted for the hybrid statistical–dynamical model is based on a Poisson regression, which has shown a skill for the prediction

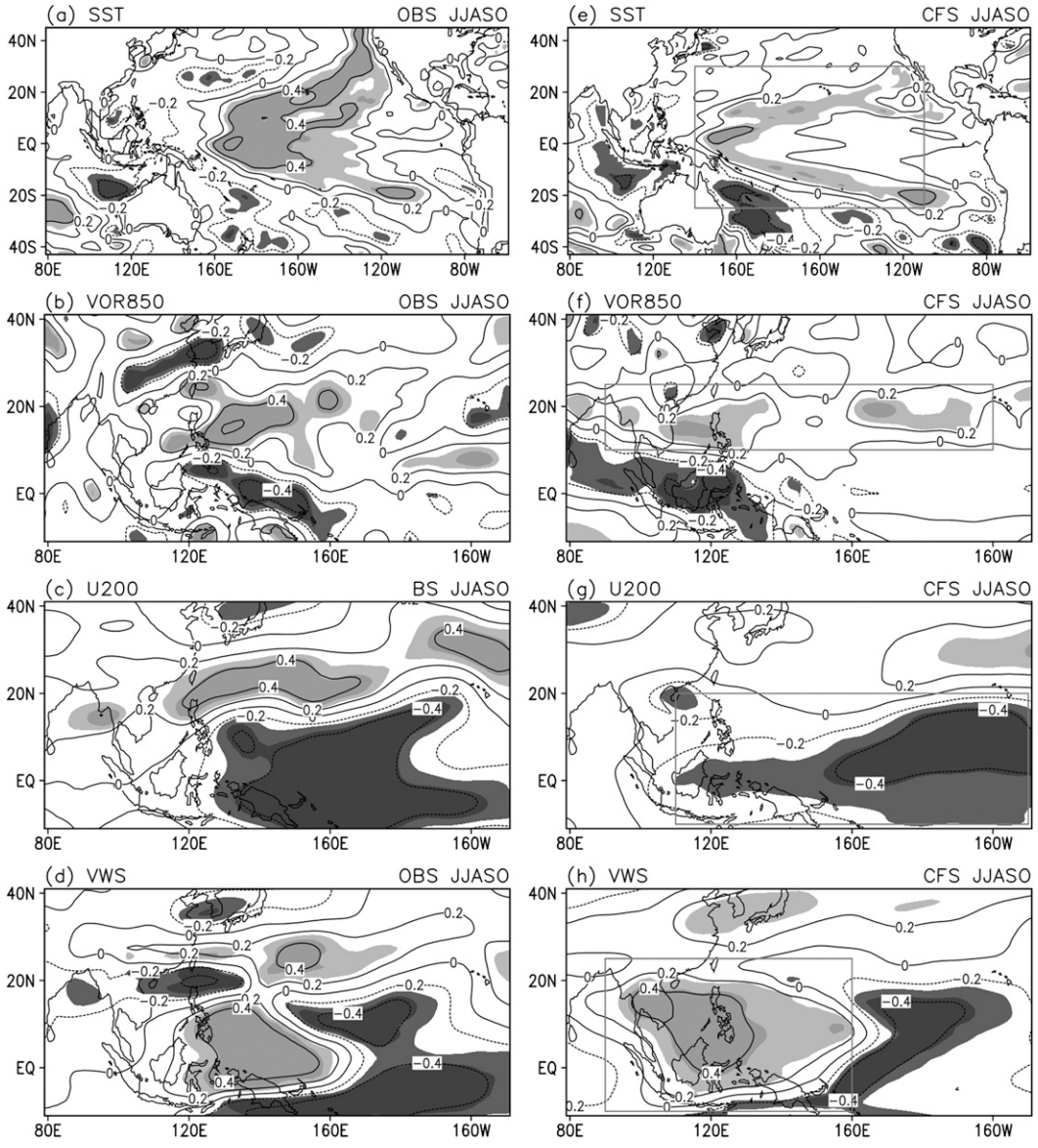

FIG. 5. As in Fig. 3, but for the TC frequency in C3.

of the TC activity (e.g., Elsner and Schmertmann 1993; McDonnell and Holbrook 2004; Chu and Zhao 2007; H.-S. Kim et al. 2010). In the Poisson regression, the expected number of events (i.e., the predictand) is assumed as the exponential function of a linear combination of predictors, expressed as

$$\tilde{y} = \exp\left(\sum_{j=1}^{k} \beta_j x_j + \beta_0\right), \tag{1}$$

where $\tilde{y}$ is the predictand (i.e., seasonal TC count), k is the number of predictors, x_j represents the predictors, β_j is the corresponding regression coefficients, and β_0 is the regression constant. The regression coefficients and constant are estimated by maximizing the likelihood of the Poisson distribution using iteration for a training period (Wilks 2006).

The variance of the Poisson distribution is fixed to the same value as its mean. In practice, the variability of target events sometimes becomes higher than the restriction of the Poisson distribution, which is called overdispersion. The overdispersion can be quantified by the dispersion parameter that measures the ratio of the variance to the mean (Tippett et al. 2011). The Poisson regression is overdispersed when the parameter is greater than 1. We check the dispersion parameters of the

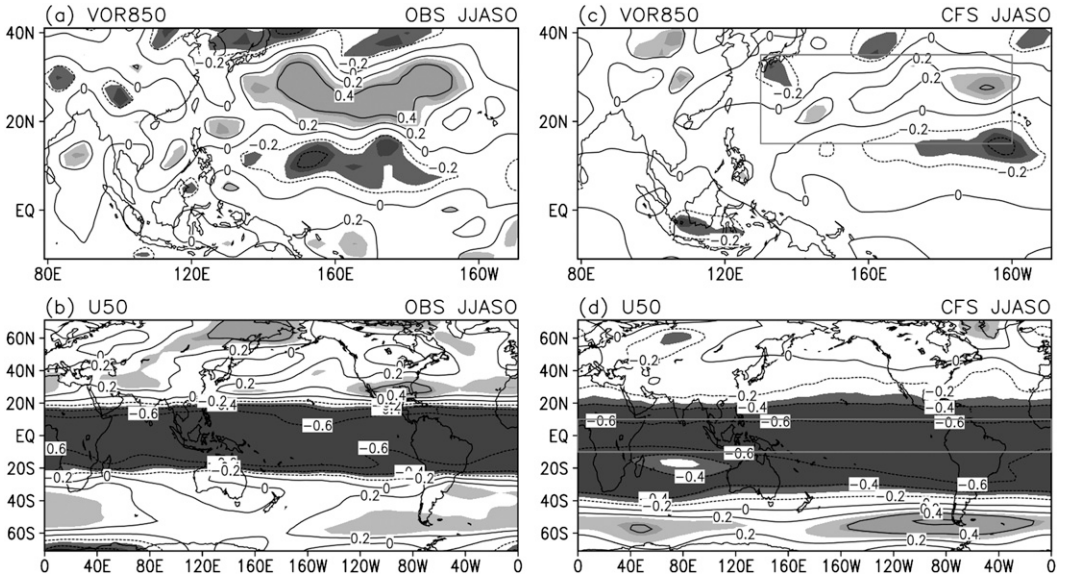

FIG. 6. As in Fig. 3, but for correlation coefficients between the TC frequency in C4 and VOR_{850} and U_{50} in (a),(b) the observations and (c),(d) NCEP CFS forecasts.

Poisson regressions for the seven patterns using the ensemble predictor sets (not shown). The results show slight overdispersion of only three ensemble cases for C2 (the dispersion parameters are 1.1 for these three cases), whereas most of the other cases do not. This ensures that the Poisson regression is suitable for the statistical prediction scheme in the hybrid statistical–dynamical model.

c. *Construction of the forecasting map of seasonal TC tracks*

The seasonal TC track density for a particular year is represented by the probability of TC tracks (P) at each grid point defined as

$$P_l(\text{lat, lon}) = \frac{N_{\text{within 5° from a grid point(lat, lon)},l}}{N_{\text{Total},l}}, \quad (2)$$

where l denotes the year index, lat and lon are the degrees of latitude and longitude, and N indicates the number of TCs (e.g., $N_{\text{Total},l}$ is the total number of TCs for a TC season of year l): P_l can be calculated using the *observed* TC tracks for all WNP grid points in year l. We can convert P_l into two probability terms using the relation based on the seven track patterns as follows:

$$N_{\text{within 5° from a grid point(lat, lon)},l} = \sum_{i=1}^{C} N_{Ci \text{ within 5° from a grid point(lat, lon)},l}, \quad (3)$$

where Ci denotes the ith pattern, and C is the number of patterns (i.e., 7). Then, the converted P_l becomes

$$P_l(\text{lat, lon}) = \sum_{i=1}^{C} \frac{N_{Ci,l}}{N_{\text{Total},l}} \times \frac{N_{Ci \text{ within 5° from grid point(lat, lon)},l}}{N_{Ci,l}} = \sum_{i=1}^{C} \frac{N_{Ci,l}}{N_{\text{Total},l}} \times P_{Ci,l}(\text{lat, lon}). \quad (4)$$

Here $N_{Ci,l}$ is the predictand of the hybrid statistical–dynamical model for Ci in year l, and $N_{\text{Total},l}$ is calculated by summing the predictands of the seven patterns; that is, $N_{\text{Total},l} = \sum_{i=1}^{C} N_{Ci,l}$. In Eq. (4), however, $P_{Ci,l}$ remains unknown because we do not know the observed probability of the year prior to the TC season. Therefore, an alternative is adopted where the climatological probabilities of the seven patterns (P_{Ci}) are substituted for $P_{Ci,l}$ (Fig. 8). Using the TC tracks of each pattern (Fig. 2), the seven P_{Ci} are calculated at a grid size of $1° \times 1°$ and applied as the basis for creating the basin-wide map of TC track density. Using Eq. (4) the spatial distribution of the TC track density for a forecasting year l ($\tilde{P}_l$) results from the sum of the climatological probability (P_{Ci}) weighted by the predicted number of TCs for the seven patterns [i.e., $\tilde{y}_{i,l}$ in Eq. (1)], which is

$$\tilde{P}_l = \sum_{i=1}^{C} \tilde{y}_{i,l} P_{Ci} \Big/ \sum_{i=1}^{C} \tilde{y}_{i,l}. \quad (5)$$

To verify this construction method using the climatological probabilities as the basis, the mean and standard deviation of the seasonal total TC track density are compared between the observed probability and the probability derived from Eq. (5) (Fig. 9). The observed

TABLE 1. (a) Correlation coefficients (COR), (b) rms errors (RMSE), and (c) mean square skill scores (MSSS) between the ensemble mean of the hindcasts and their range (maximum and minimum) for the 15 ensemble members in each cluster.

Pattern	Ensemble mean	Ensemble members	
	(a) COR		
		Max	Min
C1	0.75	0.69	0.33
C2	0.74	0.74	0.44
C3	0.72	0.65	0.23
C4	0.81	0.80	0.62
C5	0.74	0.66	0.21
C6	0.77	0.67	0.37
C7	0.71	0.68	0.49
	(b) RMSE		
		Max	Min
C1	1.30	2.01	1.46
C2	1.44	3.20	1.45
C3	1.21	1.90	1.34
C4	0.85	1.33	0.84
C5	0.96	1.71	1.05
C6	1.28	1.75	1.37
C7	1.11	1.39	1.13
	(c) MSSS		
		Max	Min
C1	0.54	0.42	−0.10
C2	0.53	0.53	−1.31
C3	0.51	0.38	−0.23
C4	0.63	0.65	0.18
C5	0.51	0.41	−0.56
C6	0.50	0.45	0.11
C7	0.49	0.46	0.19

mean (μ_{obs}, Fig. 9a) and standard deviation (σ_{obs}, Fig. 9b) are calculated using the probability of the observed seasonal TC track density during 1981–2006, whereas the model-constructed mean (μ_{model}, Fig. 9c) and standard deviation (σ_{model}, Fig. 9d) are derived from Eq. (5) by applying the observed number of seasonal TCs for Ci into $\tilde{y}_{i,l}$. It is shown that this construction method reproduces the climatological probability of the TC track density quite well, though it has a slight low bias against the observation (Fig. 9a versus Fig. 9c). On the other hand, the standard deviation of the model-constructed probability is much lower than the observed probability (Fig. 9b versus Fig. 9d), which is because the method is not based on the probabilities of the target year but instead is based on the climatological probabilities. This indicates that the developed model produces a weaker interannual variation than the observation. Therefore, it is essential to construct the final forecasting map with bias corrections for both the mean and variation. Following the correction method of Saha (2008), the standardized forecast anomaly is calculated by subtracting the model climatology from the forecasting map and then dividing it by the model standard deviation. The final forecasting map is generated by multiplying the observed standard deviation on the standardized forecast anomaly and then adding the observed mean. This procedure is summarized as

$$\tilde{P}_l \cong \left(\frac{\tilde{P}_l - \mu_{\text{model}}}{\sigma_{\text{model}}}\right)\sigma_{\text{obs}} + \mu_{\text{obs}}. \quad (6)$$

4. Validation

a. *Cross-validation test for the hybrid statistical–dynamical models*

A common method of verifying the prediction method is to apply a cross-validation test for the dataset in hand. Because the interannual variation of the seasonal TC frequency in each cluster is almost independent from year to year, it is appropriate to apply the leave-one-out cross-validation method (e.g., Gray et al. 1992; Chu et al. 2007). Once the forecasting target year is specified, the regression models for the track patterns are developed using the remaining years of the data as the training dataset. Then, the predictors for the target year from each track pattern serve as inputs for the regression models to yield the predicted TC frequencies for the target year. This process is repeated from 1981 to 2006.

Figure 10 shows the hindcasts for the seven patterns from the leave-one-out cross validations that were performed using the 15 NCEP CFS ensemble forecasts. The 15 ensemble members (gray lines) generally fluctuate in accordance with the observed variations (dashed lines) for all the patterns, though significant errors are found in many years. This causes the ensemble means (solid black lines) to be better correlated with the observations with much lower errors compared to the individual members, supporting the better skill of the ensemble mean in the statistical prediction (Kwon et al. 2007). For the purpose of the quantitative assessment of the ensemble means of 15 hindcasts, Table 1 lists their correlation coefficients (COR), rms errors (RMSE), and the mean square skill scores (MSSS) with the observed frequencies and their ranges (i.e., maximum and minimum values). The RMSE and MSSS are defined from the mean square error (MSE) as follows:

$$\text{RMSE} = \left(\text{MSE}_{\text{model}}\right)^{1/2} = \left[\frac{1}{n}\sum_{l=1}^{n}\left(y_l^{\text{obs}} - \tilde{y}_l\right)^2\right]^{1/2}, \quad (7)$$

and

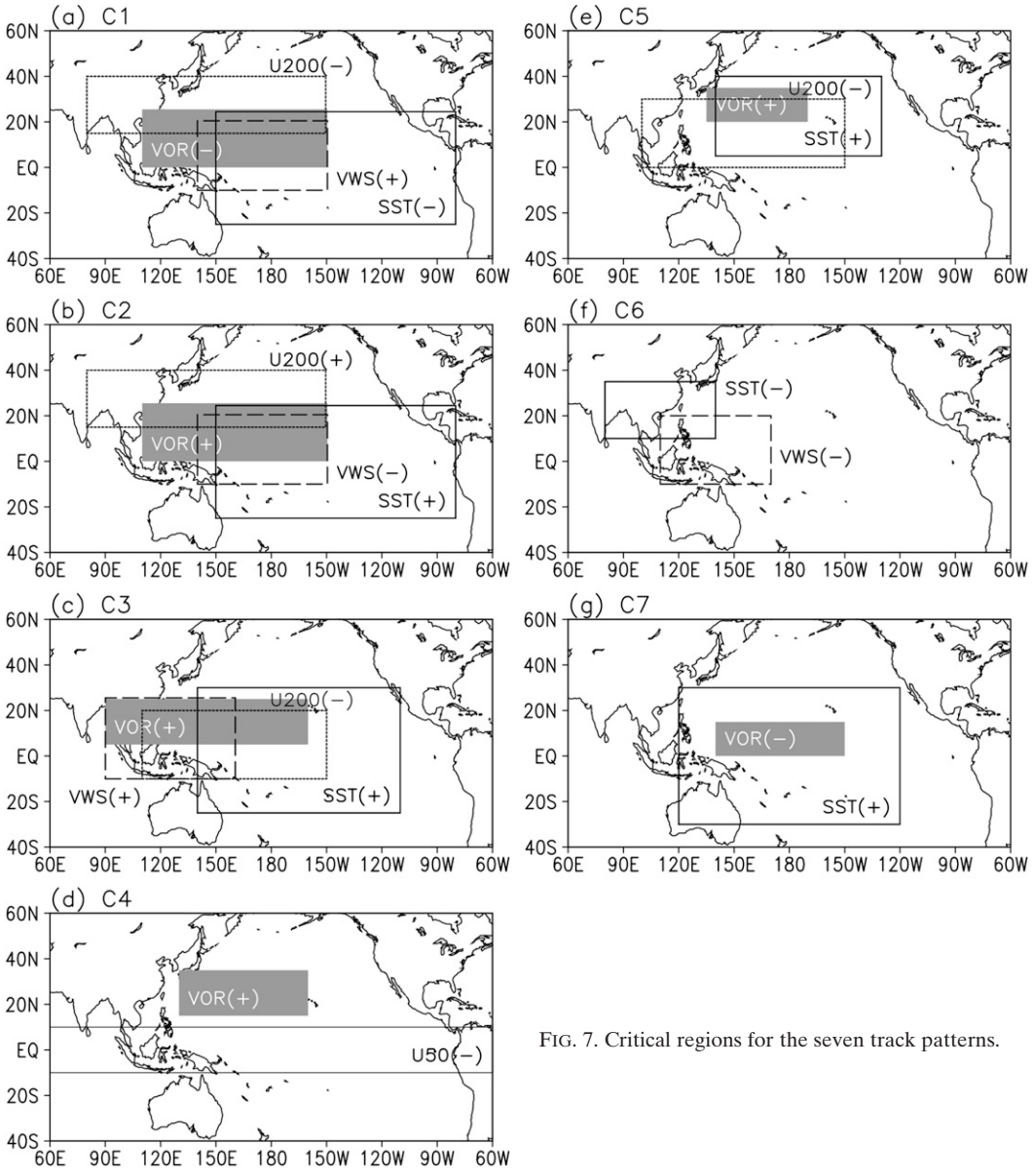

FIG. 7. Critical regions for the seven track patterns.

$$\mathrm{MSSS} = 1 - \frac{\mathrm{MSE}_{\mathrm{model}}}{\mathrm{MSE}_{\mathrm{obs}}} = 1 - \frac{\frac{1}{n}\sum_{l=1}^{n}(y_l^{\mathrm{obs}} - \tilde{y}_l)^2}{\frac{1}{n}\sum_{l=1}^{n}(y_l^{\mathrm{obs}} - \bar{y}^{\mathrm{obs}})^2}, \tag{8}$$

where n is the number of years, y_l^{obs} and $\tilde{y}_l$ are the observed TC frequency and the ensemble mean of the hindcast TC frequencies for an lth year, respectively, and $\bar{y}_l^{\mathrm{obs}}$ is the observational mean. The MSSS represents the ratio between the reduction in the MSE of the predictions of the model and the MSE of the references from the climatology (World Meteorological Organization 2002). The COR for ensemble mean are moderately high ranging from 0.71 to 0.81, and the RMSEs are around one (0.85 to 1.44). The MSSS are higher than 0.49, indicating a skill improvement of at least 50% for the models over the climatology-based reference forecasts. The indices for the ensemble mean show more skillful predictability, which is obviously because the prediction uncertainty becomes smaller in the ensemble forecast compared to the single prediction (Kwon et al. 2007). All of these statistics indicate good skill of the hybrid statistical–dynamical model. Among the seven models, the model for C4 shows the most skillful hindcasts

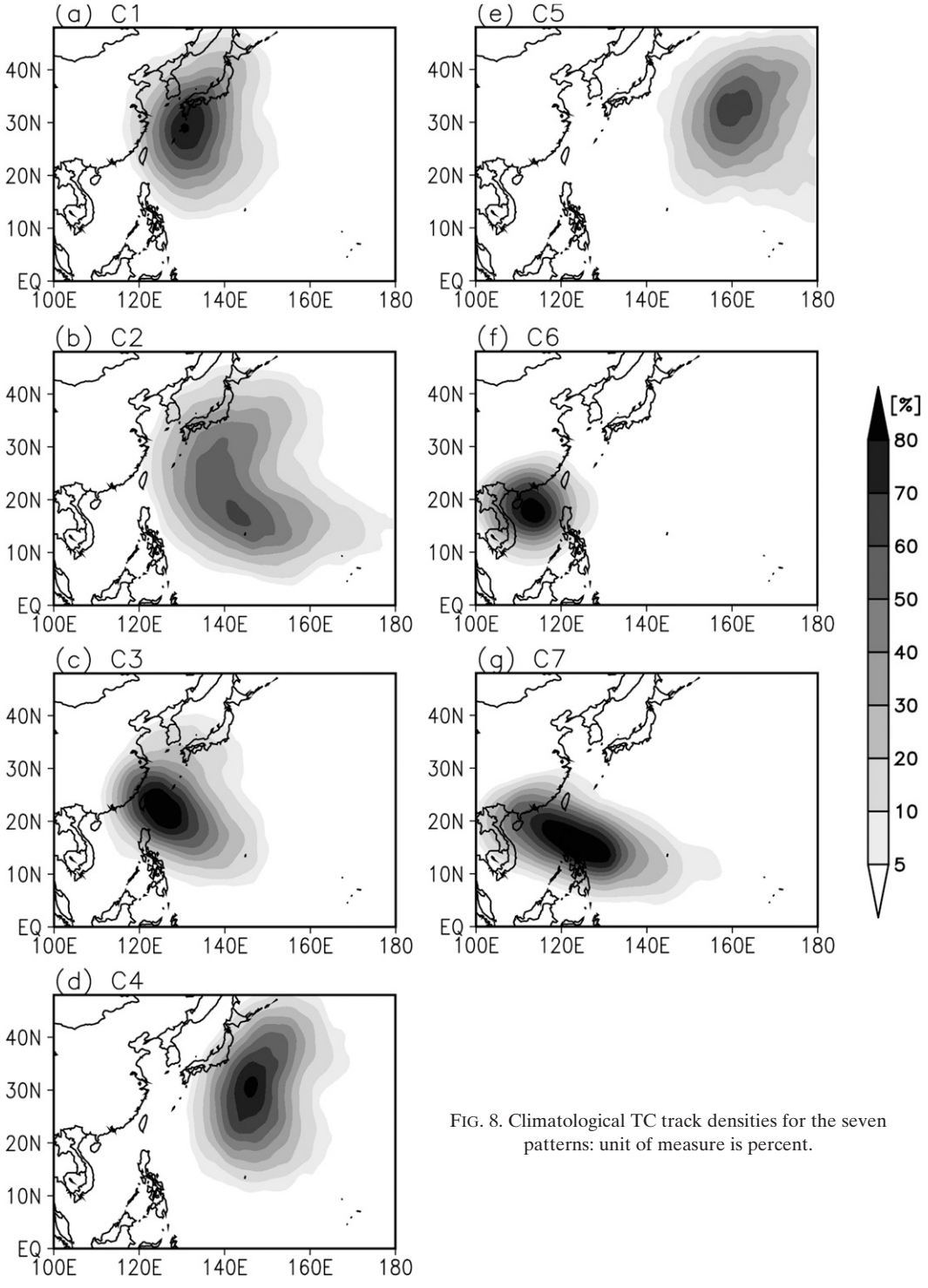

FIG. 8. Climatological TC track densities for the seven patterns: unit of measure is percent.

despite the fact that it is based on only two predictors (Fig. 10d). This implies that the QBO is a key predictor for C4 in the WNP (Ho et al. 2009b). However, for the basinwide TC frequency, the QBO is not deemed as a necessary predictor (Camargo and Sobel 2010).

b. Validation for final forecasting map: The best and the worst hindcast years

Using the ensemble mean of the 15 hindcast members, the spatial probability of seasonal TC track density is

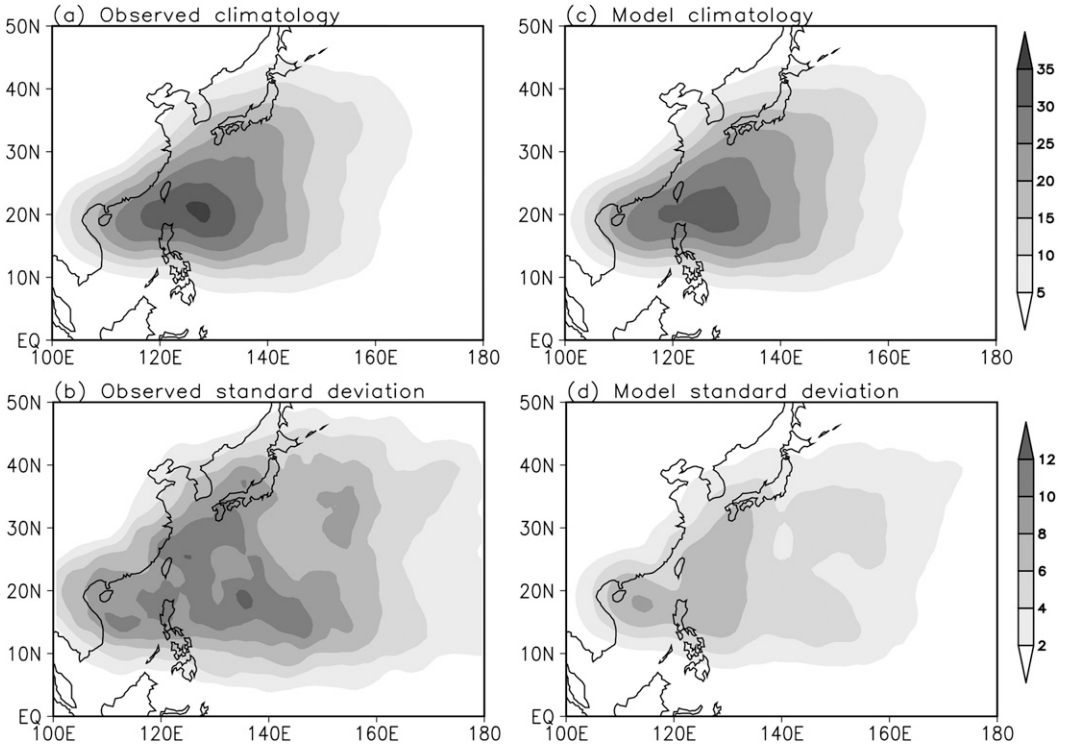

FIG. 9. Mean and standard deviation of the observed and constructed probability of the seasonal TC track density during the period 1981–2006: units of measure are percent.

produced for the TC season of each year based on the construction method described in section 3c. Among these, the 5 years that show the best (worst) hindcast are presented in Fig. 11 (Fig. 12). These years are selected based on the anomaly pattern correlation (shown in the bottom-right corner of each panel) between the observed track density (left column in Figs. 11 and 12) and model-constructed track density (middle column in Figs. 11 and 12). Also shown are the TC track densities produced using the observed TC frequencies in the seven clusters. This assumes that the hybrid statistical–dynamical model perfectly predicts the observed TC frequencies of the seven patterns (hereafter ''perfect reconstruction.'' right column in Figs. 11 and 12). The perfect reconstruction provides the upper limit of the track-pattern-based model. In these figures, the total fields of the seasonal probability are displayed with contours and their anomalies are overlapped with shading.

The hindcast maps for the skillfully predicted years show the feasibility of the track-pattern-based model to predict the anomalous spatial pattern of the seasonal TC tracks (Fig. 11). Although the microscopic view on the gridpoint values discloses the discrepancies between the estimated values and the observed values, the hindcast maps reproduce the key anomalous patterns well—that is, the west concentration pattern (i.e., high activity in the South China Sea) in 1983 (Figs. 11a and 11f) and 1995 (Figs. 11c and 11h), the bifurcate pattern (i.e., one to the South China Sea and another to the east ocean of Japan) in 1984 (Figs. 11b and 11g), the east concentration pattern (i.e., high activity east of 130°E) in 1997 (Figs. 11d and 11i), and the centralized pattern (i.e., toward East Asia through the East China Sea) in 2004 (Figs. 11e and 11j). The maps of the perfect reconstruction show the upper skill limit of the model (Figs. 11k–o). The perfect reconstruction generally shows better skill than the hindcasts. This suggests that a better skill can be achieved provided the prediction of the TC frequency is more accurate. For example, the low skill of the anomalous TC track density in the vicinity of the Philippines (Figs. 11f, 11h, and 11j) can be improved by enhancing the forecasting skill for each pattern (Fig. 11k, 11m, and 11o). It must be noted that the TC track density cannot be perfectly predicted even if the seasonal TC counts in the seven clusters are perfectly predicted. This limitation is inevitable because the final map is constructed using the climatological TC track density.

The track-pattern-based model shows poor performance in predicting the anomalous TC track density for some years (Fig. 12). There are two sources for this poor prediction. While the first source comes from the prediction based on the finite number of patterns, the second

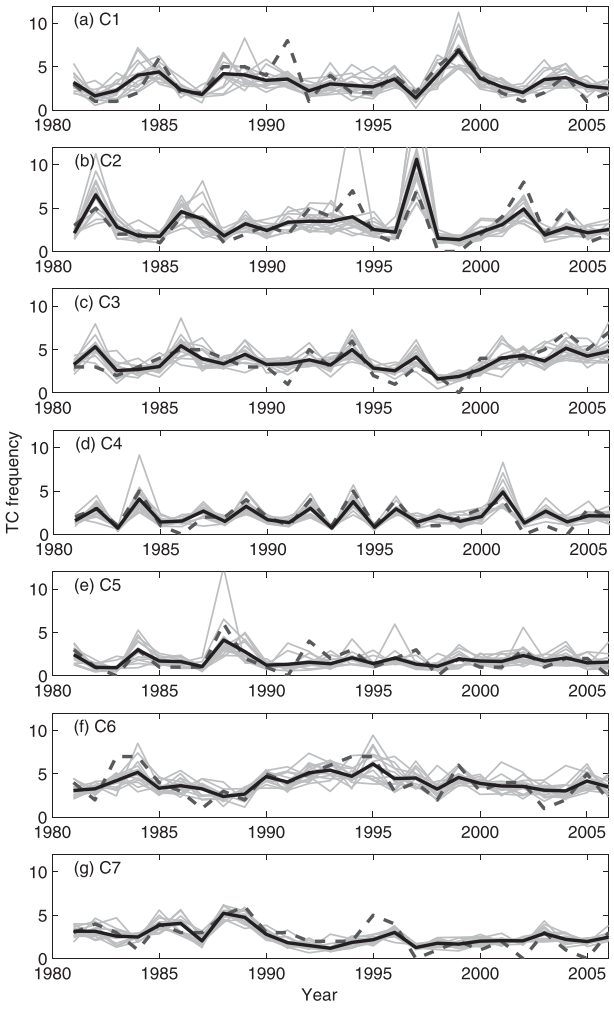

FIG. 10. Observations (dark dashed line), 15 ensemble members (gray lines), and the ensemble mean (dark solid line) of the hindcast of the hybrid dynamical prediction model for the period 1981–2006.

source comes from the innate limitation of the statistical–dynamical prediction technique itself. Although the two sources always appear together when the model prediction fails, we may classify the worst hindcast years into two types: type-1 error, which is related more to the first source, and type-2 error, which is related more to the second source. The type-1 error may include 1989, 1990, and 1993 in that even the perfect reconstruction barely produces the observed anomalous TC track density (Figs. 12k–m).[4] After careful checks of the seasonal TC tracks, we notice that most tracks in those years travel along the boundary of the seven patterns, which accordingly results in the degradation of the model based only on the seven patterns.[5] The climatology-based seven patterns are not always sufficient to cluster the seasonal tracks of individual years and outliers do exist; therefore, the prediction based on the fixed patterns can fail in those years. In contrast, years 2000 and 2002 can be classified as type-2 error because the perfect model substantially enhances the anomaly pattern correlation (Figs. 12n and 12o). In case of a type-2 error, it is no wonder that the improvement of the hybrid statistical–dynamical model may lead to a better skill in the final forecasting map. In addition to the perfect reconstruction test, we try producing the hindcast using the predictors from the reanalysis datasets to examine what happens if the dynamical model forecasts are perfect, that is, identical to the observation (not shown). Interestingly, the results do not show significant skill improvement of final forecasting map. This suggests that the type-2 error mainly originates from the statistical regression rather than the dynamic forecasts.

c. *Comparison with the ENSO–reference forecast model*

To confirm the superiority of the track-pattern-based model, we compare the forecasts by the track-pattern-based model with the reference forecasts based on the respective climatological TC track densities of different ENSO phases. That is, this ENSO-reference forecast model issues the climatology of track pattern for El Niño (La Niña) as the reference forecast for the target years if the NCEP CFS predicts the target years to be El Niño (La Niña). The ENSO-related years are selected based on the Niño-3.4 index during the TC season. El-Niño years are 1982, 1987, 1991, 1994, 1997, 2002, and 2004; La Niña years are 1984, 1985, 1988, 1995, 1998, 1999, and 2000; and the remaining years are neutral.

Figure 13 shows the mean and standard deviation of the anomaly pattern correlation coefficients between the observations and the hindcasts of the track-pattern-based model and the ENSO-reference model for all years: El Niño, La Niña, and neutral years. It is shown that the track-pattern-based model improves predictability compared to the ENSO–reference forecast based on the climatology. The mean correlation of the hindcasts by the track-pattern-based model is 0.44, while it is only 0.22 for those by the ENSO-reference model. This skill improvement relative to the reference model can be obtained for El Niño and neutral years rather

[4] The perfect reconstruction forcibly removes the second source.

[5] In other words, many data objects (i.e., TC tracks) in these years show low membership coefficients (a belongingness measure of an object into a cluster yielded by the fuzzy *c*-means clustering; Kim et al. 2011) in any of the seven clusters.

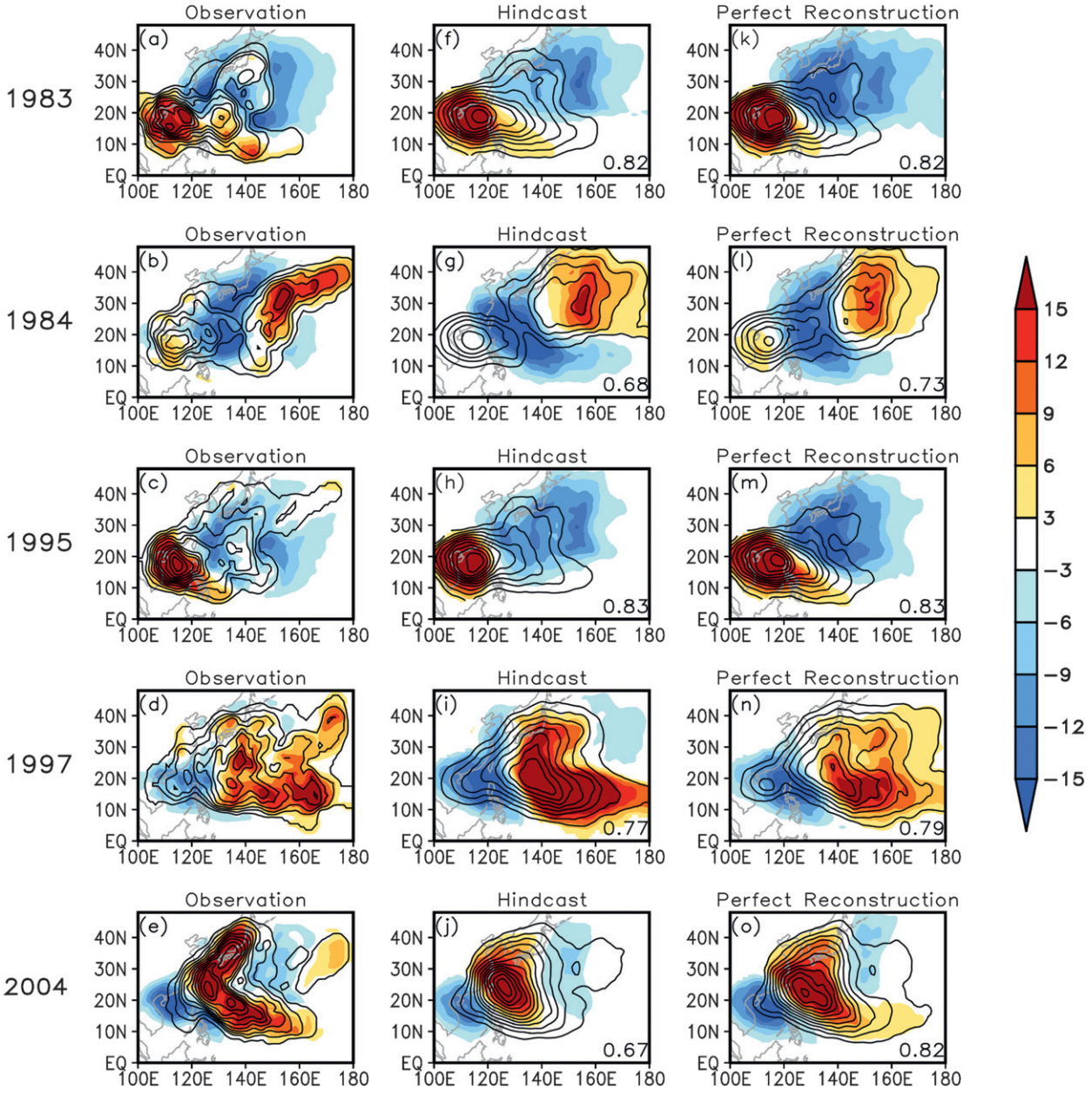

FIG. 11. Selected cases for the final forecasting map of the TC track density for 5 years with the most skillful hindcasts: (left column) Observation, (middle column) maps constructed from the hindcast results of the hybrid statistical–dynamical model, and (right column) maps constructed using the observed TC frequency in the seven patterns. Also shown are the seasonal means of the probability of the TC tracks (contours) and their anomalies (shading). Unit of measure is percent, contour interval is 5%, and the zero line is omitted. The pattern correlation coefficient with the observation is shown in the bottom-right corners.

than La Niña years. In fact, the TC track density shows large interannual variations even in a same ENSO phase (not shown, though it is seen in Fig. 11, which presents two El Niño years of 1997 and 2004 and two La Niña years of 1984 and 1995). As the track-pattern-based model uses the seven bases to construct the TC track density, it is skillful in reproducing the various spatial patterns of TC track density compared to the ENSO-reference forecast model.

It is also notable that the forecast skills for the ENSO-related years are higher than those for the neutral years. It should be noted that all of the skillful hindcast years shown in Fig. 11 are the ENSO-related years, whereas three of the 5 worst hindcast years in Fig. 11 are the

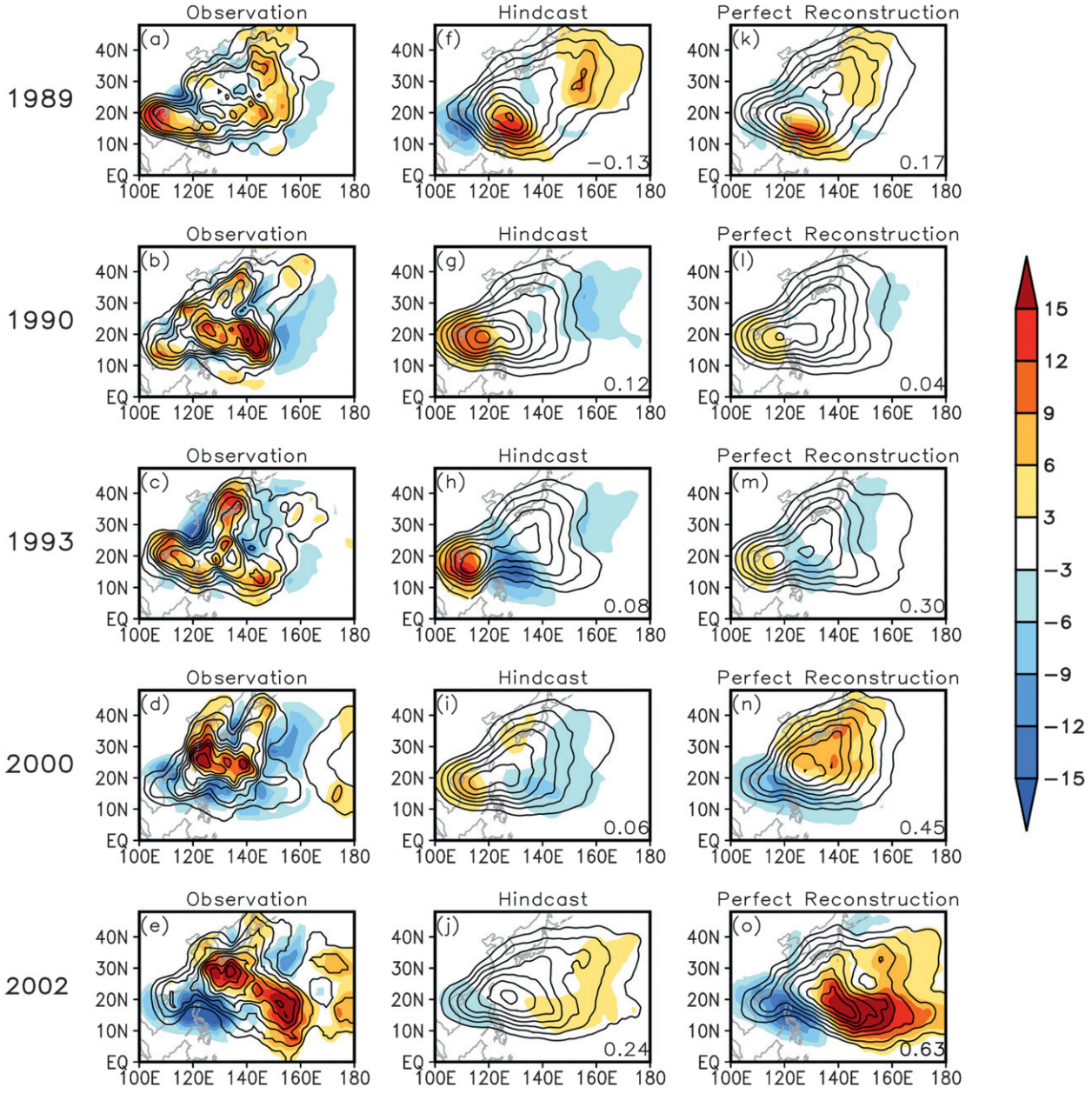

FIG. 12. As in Fig. 10, but for 5 years among the worst hindcasts.

neutral years. Relative to El Niño, the La Niña years show a slightly higher skill, although their standard deviation is correspondingly larger. The prediction skill in the perfect model also shows more improvement for the ENSO-related years. Meanwhile, the mean of the anomaly pattern correlations for the neutral years shows relatively low values and that for the perfect reconstruction is still low, suggesting that many of the neutral years may be included in the type-1 error. These differences in the prediction skill between the ENSO and the neutral years likely originate from the characteristics of the basic track patterns. As mentioned in section 3c, the ENSO-related variations are most strongly reflected in C1–C3, which result in the better performance of the model during the El Niño or La Niña years.

5. Concluding remarks

This study has introduced a novel hybrid statistical–dynamical model to predict the spatial distribution of the TC track density over the entire WNP basin. This model consists of two main steps. In the first step, the TC

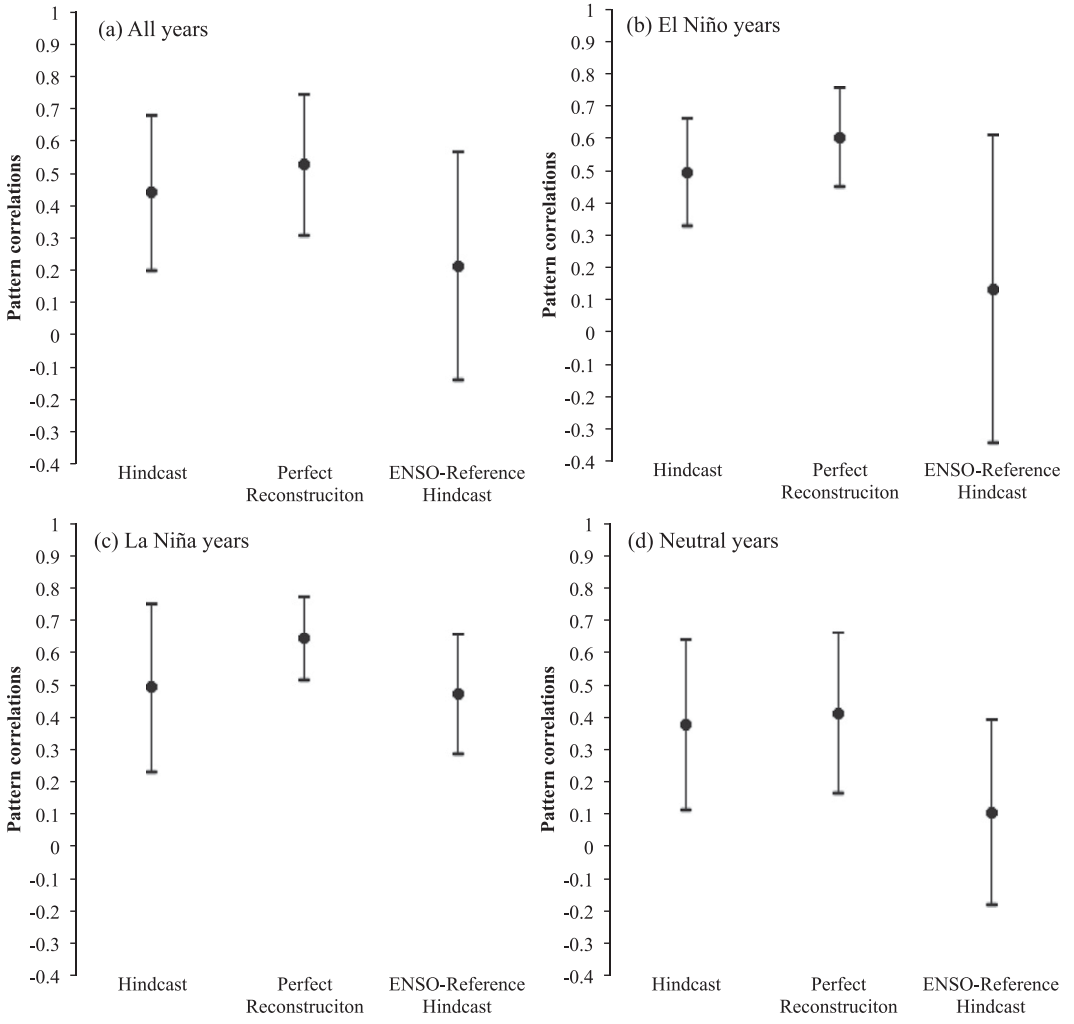

FIG. 13. Mean (solid dot) and standard deviation (range bar) of the anomaly pattern correlation coefficients between the observed and the model-constructed TC track density for (a) all years, (b) El Niña, (c) La Niña, and (d) neutral years.

frequencies of seven track patterns are predicted separately. Next, the final forecasting map is constructed by combining the prediction results of each pattern. Based on these procedures (Fig. 1), this model is named the ''track-pattern-based model.''

The prerequisite of the track-pattern-based model is classified track patterns; therefore, the basic seven track patterns were obtained by applying the fuzzy *c*-means clustering algorithm to the historical TC tracks over the WNP (Kim et al. 2011; Fig. 2). Then, the hybrid statistical–dynamical models for predicting the seasonal TC frequency of each pattern were developed using the NCEP CFS retrospective forecasts. Through correlation analyses between the seasonal TC frequencies for each pattern and concurrent seasonal environmental parameters obtained from the NCEP CFS forecasts for the period 1981–2006, the critical regions were identified as the predictors (Figs. 3, 5, 6 and 7). Thereafter, the Poisson regression models for each pattern were developed using the predictors obtained from the 15 NCEP CFS ensemble forecasts. Next, the seasonal TC track density was obtained by assembling the climatological probability of the TC tracks for the seven patterns weighted by the predicted number of TCs for each pattern [Eq. (6)]. Finally, biases in the mean and standard deviation of forecast TC track density are corrected to yield more reliable forecast [Eq. (7)].

Using 15 ensemble predictor sets for each pattern, we computed the hindcasts for the period 1981–2006 through leave-one-out cross validations. The results show that the predictions using each ensemble member have large errors but their ensemble means have skillful predictability

(Fig. 10 and Table 1). The model-constructed TC track density using the hindcasts for the seven patterns reasonably reproduces the seasonal distribution of the TC tracks in some years (Fig. 11), but not in others (Fig. 12). The reproduction of the seasonal TC track density was more skillful during the ENSO-related seasons because the basic track patterns used in the model capture the ENSO-related anomalous track patterns well (Fig. 13).

The track-pattern-based can predict the TC track density covering the entire WNP basin. This is advantageous over the previous studies that make predictions over limited areas of the basin or treat TC variations over the vast WNP basin by a single number. Recently, several studies attempted to predict the seasonal TC activity using high-resolution dynamic models (e.g., Camargo and Barnston 2009). However, dynamical prediction for TC tracks on a seasonal time scale still represents a challenge. The present study shows that the spatial distribution of the seasonal TC tracks can be predicted using a statistical technique without a high-resolution model that resolves the TC trajectory. The developed track-pattern-based model can compete with the high-resolution dynamic forecast of the seasonal TC tracks. Moreover, the NCEP CFS provides operational seasonal forecasts on a daily basis via an Internet ftp site (ftp://ftpprd.ncep.noaa.gov/pub/data1/nccf/com/cfs/prod/). With this data, the model can be directly applied as an operational seasonal prediction tool. We anticipate that the developed model can be used as an operational tool for forecasting tasks in TC-prone countries over the WNP.

Acknowledgments. This work was funded by the Korea Meteorological Administration Research and Development Program under Grant CATER 2012-2040. J.-H. Kim was supported by the National Science Council of Taiwan Grant NSC99-2811-M-002-076. Thanks are due to May Izumi of SOEST, University of Hawaii, for her editorial assistance. We appreciate the NCEP CPC and Wanqiu Wang for providing the CFS retrospective forecast datasets. We are thankful to three anonymous reviewers for their constructive suggestions.

REFERENCES

Ashok, K., S. K. Behera, S. A. Rao, H. Weng, and T. Yamagata, 2007: El Niño Modoki and its possible teleconnection. *J. Geophys. Res.,* **112,** C11007, doi:10.1029/2006JC003798.

Camargo, S. J., and A. G. Barnston, 2009: Experimental dynamical seasonal forecasts of tropical cyclone activity at IRI. *Wea. Forecasting,* **24,** 472–491.

——, and A. H. Sobel, 2010: Revisiting the influence of the quasi-biennial oscillation on tropical cyclone activity. *J. Climate,* **23,** 5810–5825.

——, M. Ballester, A. G. Barnston, P. Koltzbach, P. Roundy, M. A. Saunders, F. Vitart, and M. C. Wheeler, 2006: Short-term climate (seasonal and intra-seasonal) prediction of tropical cyclone activity and intensity. *Proc. Sixth Int. Workshop on Tropical Cyclones (IWTC-VI),* San José, Costa Rica, WMO, TMRP 72, 493–499.

——, A. W. Robertson, S. J. Gaffney, P. Smyth, and M. Ghil, 2007: Cluster analysis of typhoon tracks. Part I: General properties. *J. Climate,* **20,** 3635–3653.

Chan, J. C. L., J.-E. Shi, and C. M. Lam, 1998: Seasonal forecasting of tropical cyclone activity over the western North Pacific and the South China Sea. *Wea. Forecasting,* **13,** 997–1004.

——, ——, and K. S. Liu, 2001: Improvements in the seasonal forecasting of tropical cyclone activity over the western North Pacific. *Wea. Forecasting,* **16,** 491–498.

Choi, K.-S., D.-W. Kim, and H.-R. Byun, 2009: Statistical model for seasonal prediction of tropical cyclone frequency around Korea. *Asia-Pac. J. Atmos. Sci.,* **45,** 21–32.

Chu, P.-S., and X. Zhao, 2007: A Bayesian regression approach for predicting seasonal tropical cyclone activity over the central North Pacific. *J. Climate,* **20,** 4002–4012.

——, ——, C.-T. Lee, and M.-M. Lu, 2007: Climate prediction of tropical cyclone activity in the vicinity of Taiwan using the multivariate least absolute deviation regression method. *Terr. Atmos. Ocean. Sci.,* **18,** 805–825.

——, ——, C.-H. Kim, H.-S. Kim, M.-M. Lu, and J.-H. Kim, 2010: Bayesian forecasting of seasonal typhoon activity: A track-pattern-oriented categorization approach for Taiwan. *J. Climate,* **23,** 6654–6668.

Davis, C. E., J. E. Hyde, S. I. Bangdiwala, and J. J. Nelson, 1986: An example of dependencies among variables in a conditional logistic regression. *Modern Statistical Methods in Chronic Disease Epidemiology,* S. H. Moolgavkar and R. L. Prentice, Eds., Wiley, 140–147.

Elsner, J. B., and C. P. Schmertmann, 1993: Improving extended-range seasonal predictions of intense Atlantic hurricane activity. *Wea. Forecasting,* **8,** 345–351.

——, and T. H. Jagger, 2006: Prediction models for annual U.S. hurricane counts. *J. Climate,* **19,** 2935–2952.

Gray, W. M., 1984: Atlantic seasonal hurricane frequency. Part II: Forecasting its variability. *Mon. Wea. Rev.,* **112,** 1669–1683.

——, C. W. Landsea, P. W. Mielke, and K. J. Berry, 1992: Predicting Atlantic basin seasonal hurricane activity 6–11 months in advance. *Wea. Forecasting,* **7,** 440–455.

——, ——, ——, and ——, 1993: Predicting Atlantic basin seasonal hurricane activity by 1 August. *Wea. Forecasting,* **8,** 73–86.

——, ——, ——, and ——, 1994: Predicting Atlantic basin seasonal hurricane activity by 1 June. *Wea. Forecasting,* **9,** 103–115.

Hess, J. C., J. B. Elsner, and N. E. LaSeur, 1995: Improving seasonal hurricane predictions for the Atlantic basin. *Wea. Forecasting,* **10,** 425–432.

Ho, C.-H., and H.-S. Kim, 2011: Reexamination of the influence of ENSO on landfalling tropical cyclones in Korea. *Asia-Pac. J. Atmos. Sci.,* **47,** 457–462, doi:10.1007/s13143-011-0030-y.

——, ——, P.-S. Chu, and J.-H. Kim, 2009a: Seasonal prediction of tropical cyclone frequency over the East China Sea through a Bayesian Poisson-regression method. *Asia-Pac. J. Atmos. Sci.,* **45,** 45–54.

——, ——, J.-H. Jeong, and S.-W. Son, 2009b: Influence of stratospheric quasi-biennial oscillation on tropical cyclone tracks in the western North Pacific. *Geophys. Res. Lett.,* **36,** L06702, doi:10.1029/2009GL037163.

Kanamitsu, M., W. Ebisuzaki, J. Woollen, S.-K. Yang, J. J. Hnilo, M. Fiorino, and G. L. Potter, 2002: NCEP–DOE AMIP-II Reanalysis (R-2). *Bull. Amer. Meteor. Soc.,* **83,** 1631–1643.

Kim, H.-M., and P. J. Webster, 2010: Extended-range seasonal hurricane forecasts for the North Atlantic with a hybrid dynamical-statistical model. *Geophys. Res. Lett.,* **37,** L21705, doi:10.1029/2010GL044792.

Kim, H.-S., C.-H. Ho, P.-S. Chu, and J.-H. Kim, 2010: Seasonal prediction of summertime tropical cyclone activity over the East China Sea using the least absolute deviation regression and the Poisson regression. *Int. J. Climatol.,* **30,** 210–219.

——, J.-H. Kim, C.-H. Ho, and P.-S. Chu, 2011: Pattern classification of typhoon tracks using the fuzzy *c*-means clustering method. *J. Climate,* **24,** 488–508.

Kim, J.-H., C.-H. Ho, and P.-S. Chu, 2010: Dipolar redistribution of summertime tropical cyclone genesis between the Philippine Sea and the northern South China Sea and its possible mechanism. *J. Geophys. Res.,* **115,** D06104, doi:10.1029/2009JD012196.

Klotzbach, P. J., and W. M. Gray, 2004: Updated 6–11 month prediction of Atlantic basin seasonal hurricane activity. *Wea. Forecasting,* **19,** 917–934.

Kwon, H. J., W.-J. Lee, S.-H. Won, and E.-J. Cha, 2007: Statistical ensemble prediction of the tropical cyclone activity over the western North Pacific. *Geophys. Res. Lett.,* **34,** L24805, doi:10.1029/2007GL032308.

Liu, K. S., and J. C. L. Chan, 2003: Climatological characteristics and seasonal forecasting of tropical cyclones making landfall along the South China coast. *Mon. Wea. Rev.,* **131,** 1650–1662.

Lu, M.-M., P.-S. Chu, and Y.-C. Lin, 2010: Seasonal prediction of tropical cyclone activity in the vicinity of Taiwan using the Bayesian multivariate regression method. *Wea. Forecasting,* **25,** 1780–1795.

McDonnell, K. A., and N. J. Holbrook, 2004: A Poisson regression model approach to predicting tropical cyclogenesis in the Australian/southwest Pacific Ocean region using the SOI and saturated equivalent potential temperature gradient as predictors. *Geophys. Res. Lett.,* **31,** L20110, doi:10.1029/2004GL020843.

Nicholls, N., 1979: A possible method for predicting seasonal tropical cyclone activity in the Australian region. *Mon. Wea. Rev.,* **107,** 1221–1224.

O'Brien, R. M., 2007: A caution regarding rules of thumb for variance inflation factors, *Qual. Quant.,* **41,** 673–690, doi:10.1007/s11135-006-9018-6.

Reynolds, R. W., N. A. Rayner, T. M. Smith, D. C. Stokes, and W. Wang, 2002: An improved in situ and satellite SST analysis for climate. *J. Climate,* **15,** 1609–1625.

Saha, S., cited 2008: Documentation of operational NCEP CFS data files. NCEP, 7 pp. [Available online at http://cfs.ncep.noaa.gov/menu/doc/.]

——, and Coauthors, 2006: The NCEP Climate Forecast System. *J. Climate,* **19,** 3483–3517.

Saunders, M. A., and A. S. Lea, 2005: Seasonal prediction of hurricane activity reaching the coast of the United States. *Nature,* **434,** 1005–1008.

Tippett, M. K., S. J. Camargo, and A. H. Sobel, 2011: A Poisson regression index for tropical cyclone genesis and the role of large-scale vorticity in genesis. *J. Climate,* **24,** 2335–2357.

Vecchi, G. A., M. Zhao, H. Wang, G. Villarini, A. Rosati, A. Kumar, I. M. Held, and R. Gudgel, 2011: Statistical–dynamical predictions of seasonal North Atlantic hurricane activity. *Mon. Wea. Rev.,* **139,** 1070–1082.

Villarini, G., G. A. Vecchi, T. R. Knutson, and J. A. Smith, 2011: Is the recorded increase in short-duration North Atlantic tropical storms spurious? *J. Geophys. Res.,* **116,** D10114, doi:10.1029/2010JD015493.

Vitart, F., and Coauthors, 2007: Dynamically-based seasonal forecasts of Atlantic tropical storm activity issued in June by EUROSIP. *Geophys. Res. Lett.,* **34,** L16815, doi:10.1029/2007GL030740.

Wang, B., and J. C. L. Chan, 2002: How strong ENSO events affect tropical storm activity over the Western North Pacific. *J. Climate,* **15,** 1643–1658.

Wang, H., J.-K. E. Schemm, A. Kumar, W. Wang, L. Long, M. Chelliah, G. D. Bell, and P. Peng, 2009: A statistical forecast model for Atlantic seasonal hurricane activity based on the NCEP dynamical seasonal forecast. *J. Climate,* **22,** 4481–4500.

Wilks, D. S., 2006: *Statistical Methods in the Atmospheric Science.* 2nd ed. Academic Press, 627 pp.

World Meteorological Organization, 2002: Standardized verification system for long-range forecasts, New attachment II-9 to the manual on the GDPFS. World Meteorological Organization Rep. WMO-No. 485, 22 pp.

Zhao, M., I. M. Held, and G. A. Vecchi, 2010: Retrospective forecasts of the hurricane season using a global atmospheric model assuming persistence of SST anomalies. *Mon. Wea. Rev.,* **138,** 3858–3868.